

Universal dimer-dimer scattering in lattice effective field theory

Serdar Elhatisari,^{1,2,*} Kris Katterjohn,^{3,†} Dean Lee,^{4,‡}
Ulf-G. Meißner,^{1,5,§} and Gautam Rupak^{3,¶}

¹*Helmholtz-Institut für Strahlen- und Kernphysik (Theorie)
and Bethe Center for Theoretical Physics, Universität Bonn, D-53115 Bonn, Germany*

²*Department of Physics, Karamanoglu Mehmet Bey University, Karaman 70100, Turkey*

³*Department of Physics & Astronomy and HPC² Center for Computational Sciences,
Mississippi State University, Mississippi State, Mississippi State 39762, USA*

⁴*Department of Physics, North Carolina State University,
Raleigh, North Carolina 27695, USA*

⁵*Institute for Advanced Simulation, Institut für Kernphysik,
Jülich Center for Hadron Physics and JARA - High Performance Computing,
Forschungszentrum Jülich, D-52425 Jülich, Germany*

(Dated: December 9, 2024)

Abstract

We consider two-component fermions with short-range interactions and large scattering length. This system has universal properties that are realized in many different fields including atomic, nuclear and particle physics. In the limit of large fermion-fermion scattering length a_{ff} and zero range interaction, all properties of the system scale proportionally with the only length scale a_{ff} . We consider the case where there are bound dimers and calculate the scattering phase shifts for the two-dimer system near threshold using lattice effective field theory. From the scattering phase shifts, we extract the universal dimer-dimer scattering length $a_{\text{dd}}/a_{\text{ff}} = 0.645(89)$ and effective range $r_{\text{dd}}/a_{\text{ff}} = -0.413(79)$.

* elhatisari@hiskp.uni-bonn.de

† kk278@msstate.edu

‡ dean.lee@ncsu.edu

§ meissner@hiskp.uni-bonn.de

¶ grupak@u.washington.edu

I. INTRODUCTION

In this work we consider the low energy scattering of two dimers, each comprised of two-component fermions. The fermion-fermion interaction is tuned to produce a single shallow bound state. In nuclear physics, large scattering lengths occur naturally in two-nucleon systems where, for example, the neutron-neutron scattering length $|a_{nn}| \sim 19$ fm is much larger than the range of the nuclear force $R \sim 1/M_\pi \sim 1.4$ fm, with M_π the pion mass. Halo nuclei such as the deuteron, boron-8, and lithium-11 with small nucleon separation energies also fall in this category. In particle physics, four-quark states such as the X(3872) have been argued to be shallow molecular states of two mesons. In atomic physics, one can reach arbitrarily close to the universal limit using an external magnetic field near a Feshbach resonance to tune the scattering length. In this case, a gas of shallow dimer states is produced at positive scattering length, and the universal properties of dimer-dimer scattering determine the energy density of the dimer gas in the dilute limit, see Ref. [1].

Low-energy scattering between two non-relativistic two-component fermions interacting with a short-range potential can be described in terms of the phase shift $\delta(p)$ that is parameterized by the effective range expansion (ERE) as a function of the relative momenta p ,

$$p \cot \delta = -\frac{1}{a_{\text{ff}}} + \frac{1}{2} r_{\text{ff}} p^2 + \mathcal{O}(p^4). \quad (1)$$

We consider the situation where the two-fermion scattering length a_{ff} is very large compared to other length scales, such as the two-fermion effective range r_{ff} . This system can be described using an effective field theory (EFT) with zero-range interactions [2, 3]. Since the two-fermion system is completely characterized by the scattering length a_{ff} , the dimer-dimer scattering is necessarily proportional to a_{ff} . Previous calculations of the dimer-dimer scattering length have found $a_{\text{dd}}/a_{\text{ff}} = 0.60 \pm 0.01$ [4, 5], $a_{\text{dd}}/a_{\text{ff}} = 0.605 \pm 0.005$ [6], and $a_{\text{dd}}/a_{\text{ff}} = 0.60$ [7]. A perturbative expansion about four space-time dimensions gives $a_{\text{dd}}/a_{\text{ff}} \approx 0.66$ [8]. But the higher-order dimer-dimer ERE parameters are much less known. The effective range has been calculated as $r_{\text{dd}}/a_{\text{ff}} \approx 0.12$ in Ref. [9], while a very rough estimate of $r_{\text{dd}}/a_{\text{ff}} \sim 2.6$ was given in Ref. [10].

In this work we calculate the low-energy dimer-dimer phase shifts from lattice EFT and extract both the dimer-dimer scattering length a_{dd} and effective range r_{dd} . The choice of our method is motivated by the fact that EFT provides a model-independent framework to carry out the calculations. By formulating the theory on a space-time lattice, we are able to perform a non-perturbative calculation with controlled systematic errors.

We organize our paper as follows. In Sec. II we introduce the continuum and lattice formulations describing the systems of two-component fermions. In Sec. III we discuss the methods for extracting the scattering information from periodic finite volumes. We present our results and analyses for the fermion-dimer and dimer-dimer scattering in Sec. IV. Then the results are summarized in Sec. V.

II. LATTICE FORMALISM

We start by describing the system of interacting two-component fermions in the continuum. The low-energy scattering is dominated by the s -wave, while higher partial waves

become more important at higher energies. In the continuum we describe the system with the following non-relativistic Hamiltonian,

$$H = \sum_s \frac{1}{2m_s} \int d^3\vec{r} \vec{\nabla} b_s^\dagger(\vec{r}) \cdot \vec{\nabla} b_s(\vec{r}) + C_0 \int d^3\vec{r} \rho_\uparrow(\vec{r}) \rho_\downarrow(\vec{r}), \quad (2)$$

where s specifies the particle species and the sum goes over all the particles (2, 3 or 4), C_0 is the interaction strength, b_s (b_s^\dagger) is the annihilation (creation) operator, and $\rho_{\uparrow,\downarrow}$ is the density operator,

$$\rho_s(\vec{r}) = b_s^\dagger(\vec{r}) b_s(\vec{r}). \quad (3)$$

We use parameters commonly used in the nuclear physics of neutrons. We work with natural units $\hbar = 1 = c$, and set the masses equal $m = m_\uparrow = m_\downarrow = 939.0$ MeV. However the final results we present are universal and do not depend on this choice of parameters. The coupling strength C_0 can be tuned according to either the two-body scattering length a_{ff} or the dimer binding energy B_{d} . In our analysis we tune it according to the binding energy B_{d} .

The ultraviolet divergences due to the zero-range interaction must be regulated in some manner. We put the system on a lattice which automatically provides the needed regularization. We denote the lattice spacing as a and write all quantities in lattice units by multiplying with the corresponding power of a to render the combination dimensionless. The tuned value of C_0 depends on the lattice spacing a . In our calculations we use an $\mathcal{O}(a^4)$ -improved lattice action where the free lattice Hamiltonian, H_0 , is defined as,

$$\hat{H}_0 = \sum_s \frac{1}{2m_s} \sum_{\hat{l}=\hat{1},\hat{2},\hat{3}} \sum_{\vec{n}} \left[\sum_{k=-3}^3 w_{|k|} b_s^\dagger(\vec{n}) b_s(\vec{n} + k\hat{l}) \right], \quad (4)$$

where $\hat{l} = \hat{1}, \hat{2}, \hat{3}$ are unit vectors in spatial directions, w_0, w_1, w_2 , and w_3 are $49/18, -3/2, 3/20$, and $-1/90$, respectively. \vec{n} denotes the lattice sites on a three-dimensional $L \times L \times L$ periodic cube. The lattice form of the potential is

$$\hat{V} = C_0 \sum_{\vec{n}} \rho_\uparrow(\vec{n}) \rho_\downarrow(\vec{n}). \quad (5)$$

The definition of the lattice theory is complete once we tune the lattice coupling C_0 to produce a two-fermion bound state with binding energy B_{d} for a value of lattice spacing a . We can then compute what happens to a multi-particle system.

In the low energy limit of this theory, three-body and higher-body interactions are irrelevant operators. Their contributions are suppressed by several powers of the lattice spacing a . Nevertheless, we find it convenient to include three-body ($3N$) and four-body ($4N$) interactions in order to verify that we can extrapolate to the same continuum limit starting from several different starting points. In the following we define the three-body potential consisting of nearest-neighbour and next-to-nearest-neighbour interactions,

$$\begin{aligned} \hat{V}_{3N} = & C_{3N}^{(1)} \sum_{\hat{e}_1=\hat{1},\hat{2},\hat{3}} \sum_{\vec{n},s} \rho_\uparrow(\vec{n}) \rho_\downarrow(\vec{n}) \rho_s(\vec{n} + \hat{e}_1) \\ & + C_{3N}^{(2)} \sum_{\substack{\hat{e}_1,\hat{e}_2=\hat{1},\hat{2},\hat{3} \\ e_2 > e_1}} \sum_{\vec{n},s} \rho_\uparrow(\vec{n}) \rho_\downarrow(\vec{n}) \rho_s(\vec{n} + \hat{e}_1 + \hat{e}_2). \end{aligned} \quad (6)$$

Similarly, we introduce the following four-body potential that consists of nearest-neighbour and next-to-nearest-neighbour interactions,

$$\begin{aligned} \hat{V}_{4N} = & C_{4N}^{(1)} \sum_{\hat{e}=\hat{1},\hat{2},\hat{3}} \sum_{\vec{n}} \rho_{\uparrow}(\vec{n}) \rho_{\downarrow}(\vec{n}) \rho_{\uparrow}(\vec{n} + \hat{e}) \rho_{\downarrow}(\vec{n} + \hat{e}) \\ & + C_{4N}^{(2)} \sum_{\substack{\hat{e}_1, \hat{e}_2=\hat{1},\hat{2},\hat{3} \\ e_2 > e_1}} \sum_{\vec{n}} \rho_{\uparrow}(\vec{n}) \rho_{\downarrow}(\vec{n}) \rho_{\uparrow}(\vec{n} + \hat{e}_1 + \hat{e}_2) \rho_{\downarrow}(\vec{n} + \hat{e}_1 + \hat{e}_2). \end{aligned} \quad (7)$$

Here the interaction strengths $C_{3N}^{(1,2)}$ and $C_{4N}^{(1,2)}$ are kept at fixed values in lattice units, which means that these interactions scale as a^5 and a^8 in physical units, and become irrelevant in the continuum limit.

III. SCATTERING PHASE SHIFT

Lüscher's finite-volume method relates the two-body energy levels in a cubic periodic box to the elastic scattering phase shifts [11, 12]. The two-body phase shifts in a periodic box of size L is related to the relative momentum of two particles, p , by the relation

$$p \cot \delta(p) = \frac{1}{\pi L} S(\eta), \quad \eta = \left(\frac{pL}{2\pi} \right)^2, \quad (8)$$

where $S(\eta)$ is the regulated three-dimensional zeta function given by,

$$S(\eta) = \lim_{\Lambda \rightarrow \infty} \left[\sum_{\vec{n}} \frac{\Theta(\Lambda^2 - \vec{n}^2)}{\vec{n}^2 - \eta} - 4\pi\Lambda \right]. \quad (9)$$

We use lattice calculations at different L to determine the values of p as input into Eq. (8), which is then evaluated to obtain the two-body scattering phase shift $\delta(p)$.

As we will discuss later, we rescale our results for the fermion-dimer and the dimer-dimer scattering parameters by the fermion-fermion scattering length, a_{ff} . In the continuum and infinite volume limits the binding energy of two fermions interacting with a zero-range interaction is related to the scattering length by $B_{\text{d}} = 1/(ma_{\text{ff}}^2)$. In this analysis we compute a_{ff} using this formula and the dimer binding energy B_{d} computed on the lattice. In order to probe lattice artifacts appearing in the two-body system, we also compute the two-fermion scattering length $a_{\text{ff}}^{\text{latt}}$ using Lüscher's finite volume method. In Fig. 1 we show the ratio of the two-fermion scattering lengths for various lattice spacings a . We note that the deviation between these two definitions of the scattering lengths are small and can be fit nicely with a polynomial in the lattice spacing a as shown Fig. 1.

We can also analyze the scattering system using Lüscher's finite volume method for a system of one or two composite objects. In the infinite volume and the continuum limits, the relative momentum p is related to the two-body energy levels $E^{(\infty)}$ as

$$E^{(\infty)} = \frac{p^2}{2\mu} - B_1, \quad (10)$$

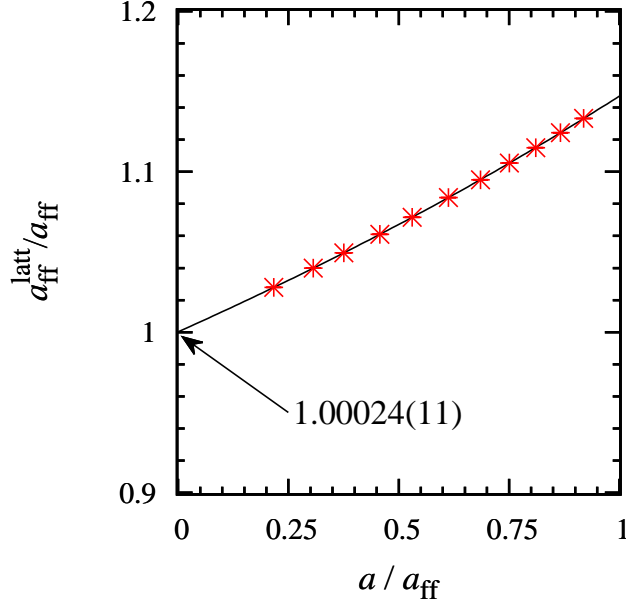


FIG. 1: The ratio of the fermion-fermion scattering lengths a_{ff} and $a_{\text{ff}}^{\text{latt}}$ versus the lattice spacing a . a_{ff} is determined from the dimer binding energy while $a_{\text{ff}}^{\text{latt}}$ is computed using Lüscher’s finite volume method.

when there is single composite object such as a dimer with infinite volume binding energy B_1 or as

$$E^{(\infty)} = \frac{p^2}{2\mu} - B_1 - B_2, \quad (11)$$

when there are two composite objects with infinite volume binding energies B_1, B_2 . μ is the two-body reduced mass. In this study, the two-body system will be either a fermion-dimer system where Eq. (10) is applicable or a dimer-dimer system where Eq. (11) is applicable.

At finite volume and nonzero lattice spacing, Eqs. (10) and (11) are modified by various effects. At non-zero lattice spacing, the reduced mass of the composite object is not exactly the same as that in continuum limit. So we compute the reduced mass μ^* by numerically calculating the dispersion relation of the composite particles in a very large $L^3 = 50^3$ box (in units of the lattice spacing) to minimize finite-volume errors. At finite volume, there is also finite volume correction to the binding energies, which in turn will depend on momentum of the composite objects. We account for these finite-volume momentum-dependent effects using finite-volume topological factors $\tau_d(\eta)$ due to the wave functions wrapping around the periodic box [13]. With these corrections Eq. (11) reads,

$$E^{(L)} = \frac{p^2}{2\mu^*} - B_1^{(L)} + \tau_1(\eta) \Delta B_1 - B_2^{(L)} + \tau_2(\eta) \Delta B_2, \quad (12)$$

where $\Delta B_i = B_i^{(L)} - B_i$. The topological factor is given by [13]

$$\tau(\eta) = \left[\sum_{\vec{k}} \frac{1}{(\vec{k}^2 - \eta^2)^2} \right]^{-1} \sum_{\vec{k}} \frac{\sum_{i=1}^3 \cos(2\pi\alpha k_i)}{3(\vec{k}^2 - \eta^2)^2}, \quad (13)$$

where $\alpha = m_1/(m_1 + m_2)$. The momentum p corresponding to the lattice volume of size L is computed by solving Eq. (12) self-consistently for the given lattice energies $E^{(L)}$ and $B_{1,2}^{(L)}$. The finite volume corrections to Eq. (10) are similar with a topological factor correction for the single composite dimer.

IV. RESULTS AND ANALYSIS

A. Fermion-dimer scattering

Before describing the main problem of dimer-dimer scattering, we first perform precision benchmarks of our lattice methods by describing fermion-dimer scattering. We consider a three-body system of two-component fermions consisting of two \uparrow and one \downarrow particles. The fermion-dimer is a nontrivial system for which the scattering parameters beyond the scattering length can be obtained using semi-analytical calculations [2, 14–16] in the continuum limit. We study the fermion-dimer system using the lattice action introduced in Sec. II.

The free Hamiltonian and two-particle interaction are defined in Eq. (4) and Eq. (5), respectively. The three-body ($3N$) potential introduced in Eq. (6) takes the following form for our three-body system,

$$\begin{aligned} \hat{V}_{3N} = & C_{3N}^{(1)} \sum_{\hat{e}_1=\hat{1},\hat{2},\hat{3}} \sum_{\vec{n}} \rho_{\uparrow}(\vec{n}) \rho_{\downarrow}(\vec{n}) \rho_{\uparrow}(\vec{n} + \hat{e}_1) \\ & + C_{3N}^{(2)} \sum_{\substack{\hat{e}_1,\hat{e}_2=\hat{1},\hat{2},\hat{3} \\ e_2 > e_1}} \sum_{\vec{n}} \rho_{\uparrow}(\vec{n}) \rho_{\downarrow}(\vec{n}) \rho_{\uparrow}(\vec{n} + \hat{e}_1 + \hat{e}_2). \end{aligned} \quad (14)$$

We perform lattice calculations using the Lanczos iterative eigenvector method and obtain the scattering state energies for the fermion-dimer systems with various values of $C_{3N}^{(1,2)}$ for the strength of the $3N$ potential and various values of the lattice spacing a . For the sake of simplicity, we set $C_{3N}^{(2)} = C_{3N}^{(1)}/2 = c_{3N}/2$. Then we use these energies in the fermion-dimer version of Eq. (12),

$$E_{\text{fd}}^{(L)} = \frac{p^2}{2\mu_{\text{fd}}^*} - B_{\text{d}}^{(L)} + \tau_{\text{d}}(\eta) \Delta B_{\text{d}}, \quad (15)$$

and then we use Eq. (8) to extract the fermion-dimer scattering phase shifts. The results are given in Fig. 2. As can be seen in the figure, the $3N$ forces have some impact on the scattering phase shift results at larger lattice spacings, while the data at small a is almost independent of the different values for $C_{3N}^{(1,2)}$. This is due to the fact that the three-body interactions are irrelevant operators and have no impact in the continuum limit.

We extract the scattering lengths and the effective ranges from the fermion-dimer scattering data shown in Fig. 2. We then perform the continuum limit extrapolations of the fermion-dimer scattering length a_{fd} and effective range r_{fd} as shown in Fig. 3. In the continuum limit extrapolation we use a polynomial which is fourth order in a/a_{ff} ,

$$F(a) = f_0 + f_1 (a/a_{\text{ff}}) + f_2 (a/a_{\text{ff}})^2 + f_3 (a/a_{\text{ff}})^3 + f_4 (a/a_{\text{ff}})^4. \quad (16)$$

We use a constrained fit which is applied to all of the data shown in Fig. 2. In the fit the continuum-limit parameter f_0 is required to be the same value for all data sets, while all other parameters are left free.

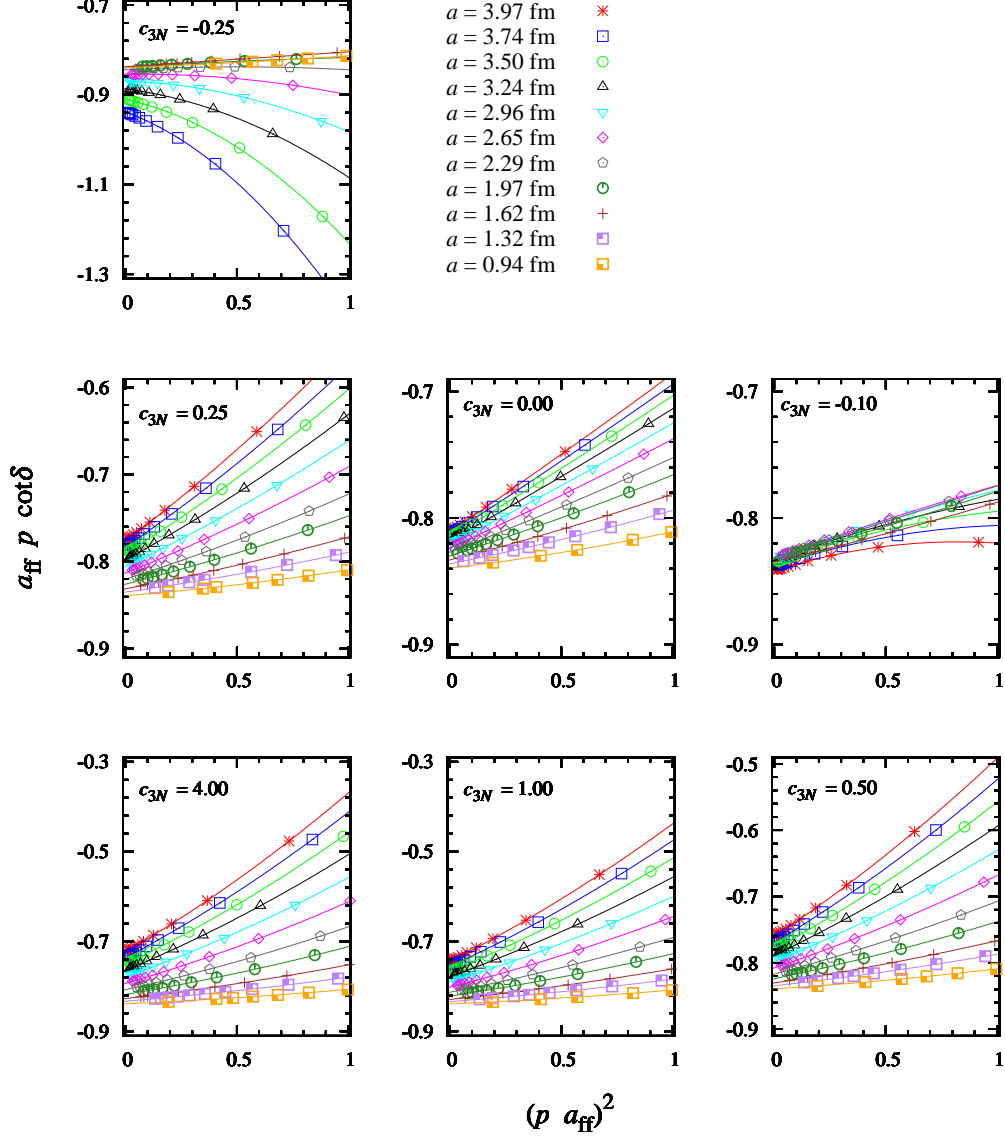


FIG. 2: The fermion-dimer scattering results for various values of lattice spacing a . We plot $a_{\text{ff}} p \cot \delta$ versus $(a_{\text{ff}} p)^2$ in the center of mass frame. Here $C_{3N}^{(1)} = c_{3N}$ and $C_{3N}^{(2)} = c_{3N}/2$.

The extrapolation fits for the scattering length and the effective range are shown in Fig. 3. The final results for the scattering parameters are $a_{\text{fd}}/a_{\text{ff}} = 1.1782(6)$ and $r_{\text{fd}}/a_{\text{ff}} = -0.0371(83)$ which are in agreement with semi-analytic continuum calculations $a_{\text{fd}}^{\text{cont.}}/a_{\text{ff}} = 1.1791(2)$ and $r_{\text{fd}}^{\text{cont.}}/a_{\text{ff}} = -0.0383(3)$ [2, 14–16]. As clearly seen in Fig. 3, the three-body forces produce corrections to the scattering parameters at higher powers of a/a_{ff} . The three-body forces produce a spread in the data which is helpful to pin down the scattering parameters in the continuum limit more accurately. The higher-body forces can also be used to empirically reduce the numerical size of corrections at larger lattice spacings.

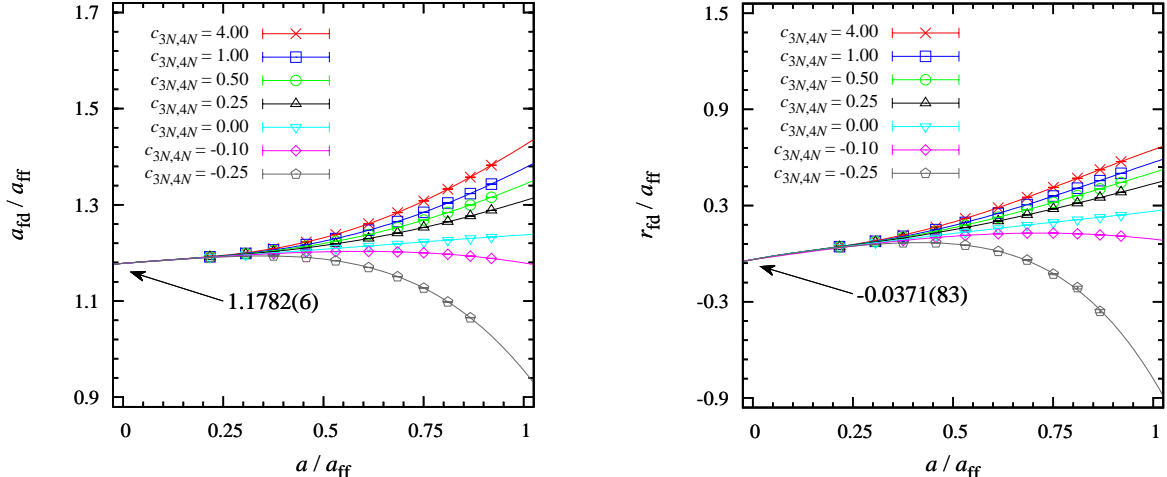


FIG. 3: (Left panel) The continuum limit extrapolation of the fermion-dimer scattering length a_{fd} . (Right panel) The continuum limit extrapolation of the fermion-dimer effective range r_{fd} . Here we set $C_{3N}^{(1)} = c_{3N}$ and $C_{3N}^{(2)} = c_{3N}/2$. The final results are $a_{\text{fd}}/a_{\text{ff}} = 1.1782(6)$ and $r_{\text{fd}}/a_{\text{ff}} = -0.0371(83)$.

B. Dimer-dimer scattering

Now we present the main topic of this paper, dimer-dimer scattering. We consider a four-body system consisting of two \uparrow and two \downarrow particles. The free lattice Hamiltonian and the two-body ($2N$) interaction are given in Eqs. (4) and (5), respectively. In addition to the $2N$ interaction, we consider the $3N$ and $4N$ interactions defined in Eqs. (6) and (7). The coefficients of the irrelevant higher body interactions are kept fixed in lattice units. As we will see, they introduce significant corrections to the scattering parameters at large lattice spacings.

We calculate the scattering state energies for the dimer-dimer system using the Lanczos iterative eigenvector method. We consider various values of $c_{3N,4N}$ for the interaction strengths of the $3N$ and $4N$ potentials and various values of the lattice spacing a . For the sake of simplicity, we set $C_{3N}^{(1)} = 2C_{3N}^{(2)} = c_{3N,4N}$ and $C_{4N}^{(1)} = 2C_{4N}^{(2)} = -3c_{3N,4N}$. We compute the relative momentum of the dimer-dimer using the scattering state energies in Eq. (12). The momentum p for each periodic box size L is used in the Lüscher's formula, Eq. (8), to extract the scattering phase shifts. We consider box sizes up to $L^3 = 12^3$. In Fig. 4 we collectively show the dimer-dimer scattering data for various values of $c_{3N,4N}$ and lattice spacing a .

The lattice results for the scattering length are shown in Fig. 5. As is clearly seen in Fig. 5, the higher-body forces produce corrections to the scattering length for large lattice spacings. However, it is clear that they become irrelevant in the continuum limit. We perform the continuum limit extrapolations using the fourth-order polynomial in Eq. (16) with continuum-limit parameter f_0 required to be the same value for all data sets. The final results for the scattering length is $a_{\text{dd}}/a_{\text{ff}} = 0.645(89)$ which is in agreement with previous numerical calculations [4–8]. We show the results from the constrained fit for the dimer-dimer scattering length in Table I.

We also extract the dimer-dimer effective range from the dimer-dimer scattering data in Fig. 4. These results are shown in Fig. 6. As can be seen clearly, without any higher-

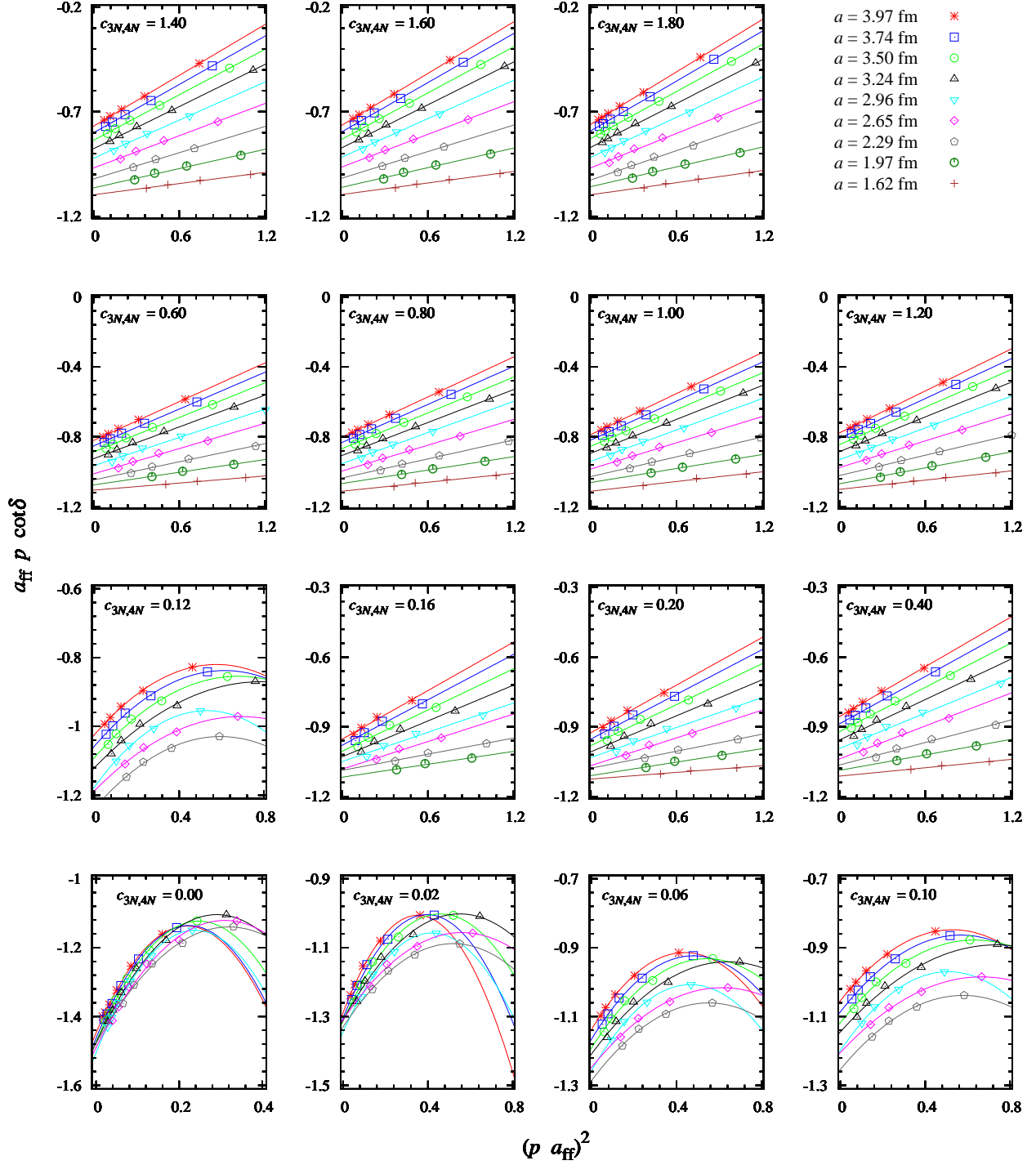


FIG. 4: The dimer-dimer scattering results for various values of lattice spacing a . We plot $a_{\text{ff}} p \cot \delta$ versus $(a_{\text{ff}} p)^2$ in the center of mass frame. Here we set $C_{3N}^{(1)} = 2 C_{3N}^{(2)} = c_{3N,4N}$ and $C_{4N}^{(1)} = 2 C_{4N}^{(2)} = -3 c_{3N,4N}$.

body interactions the dimer-dimer effective range has very large corrections at large lattice spacing, which makes the determination of the effective range very difficult. This is likely the reason for the large positive effective range found in Ref. [10]. Introducing the lattice spacing independent higher-body forces provides a spread of different data that can be used

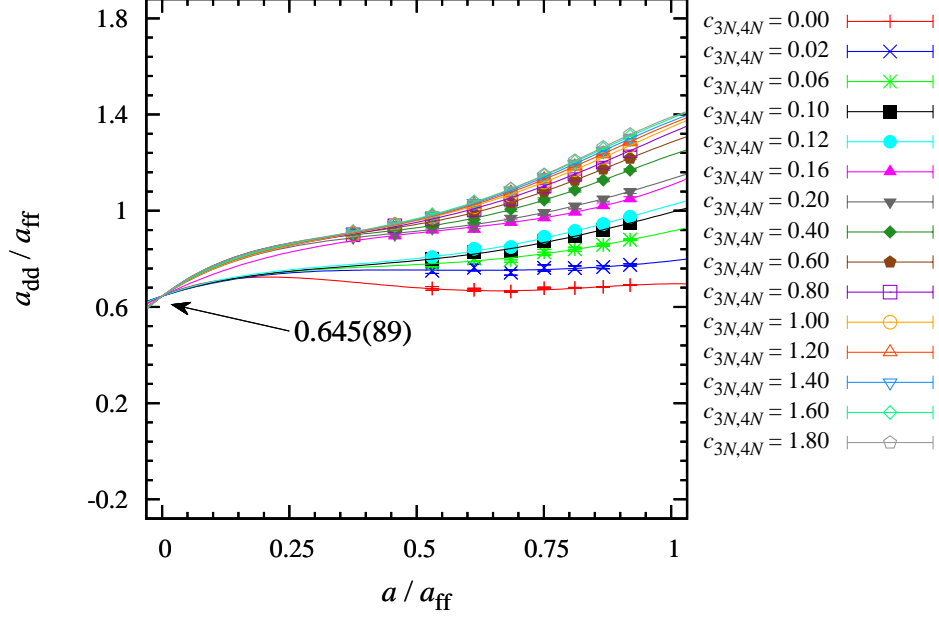


FIG. 5: The continuum limit extrapolation of the dimer-dimer scattering length a_{dd} . Here we set $C_{3N}^{(1)} = 2C_{3N}^{(2)} = c_{3N,4N}$ and $C_{4N}^{(1)} = 2C_{4N}^{(2)} = -3c_{3N,4N}$. The final result is $a_{\text{dd}}/a_{\text{ff}} = 0.645(89)$.

TABLE I: The results from the constrained fit for the dimer-dimer scattering length.

$c_{3N,4N}$	$f_0 = a_{\text{dd}}/a_{\text{ff}}$	f_1	f_2	f_3	f_4
0.00	0.645±0.089	0.908±0.529	-3.312±1.254	4.091±1.321	-1.636±0.510
0.02		0.682±0.731	-1.484±2.434	1.268±3.125	-0.319±1.360
0.06		0.724±0.694	-1.686±2.239	1.821±2.840	-0.590±1.228
0.10		0.715±0.676	-1.666±2.141	2.013±2.695	-0.714±1.161
0.12		0.778±0.664	-1.907±2.079	2.404±2.610	-0.896±1.124
0.16		1.047±0.694	-1.494±2.270	0.888±3.026	0.021±1.384
0.20		1.383±0.636	-2.983±1.738	3.103±2.092	-1.016±0.916
0.40		1.644±0.626	-4.218±1.660	5.111±1.928	-1.950±0.816
0.60		1.626±0.617	-4.145±1.594	5.192±1.795	-2.033±0.738
0.80		1.428±0.609	-3.294±1.555	4.113±1.727	-1.568±0.700
1.00		1.411±0.598	-3.215±1.504	4.085±1.651	-1.578±0.661
1.20		1.488±0.602	-3.609±1.488	4.755±1.594	-1.919±0.623
1.40		1.546±0.596	-3.892±1.461	5.228±1.556	-2.155±0.607
1.60		1.519±0.595	-3.757±1.456	5.063±1.546	-2.085±0.601
1.80		1.642±0.593	-4.385±1.459	6.020±1.563	-2.532±0.612

to determine the effective range more accurately. We also find that the higher-body forces can be used to empirically cancel large lattice spacing corrections to the dimer-dimer effective range. The higher-body forces introduced here are important in improving the accuracy of the dimer-dimer effective range calculation.

The continuum limit extrapolation of the effective range is shown in Fig. 6. Given the greater noise in the effective range data points, for this analysis we use a third-order poly-

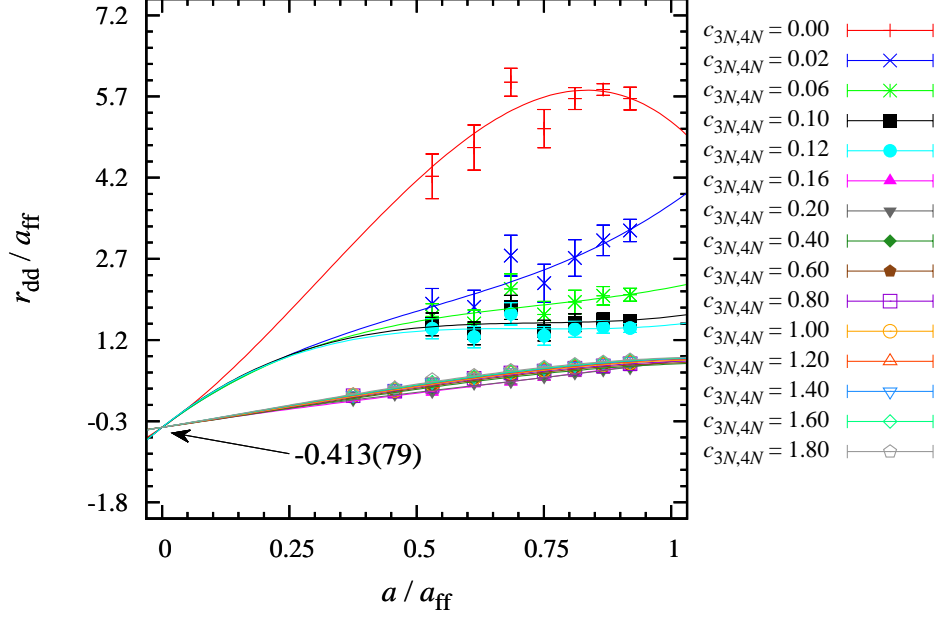


FIG. 6: The continuum limit extrapolation of the dimer-dimer effective range r_{dd} . Here we set $C_{3N}^{(1)} = 2C_{3N}^{(2)} = c_{3N,4N}$ and $C_{4N}^{(1)} = 2C_{4N}^{(2)} = -3c_{3N,4N}$. The final result is $r_{\text{dd}}/a_{\text{ff}} = -0.413(79)$.

nomial in a/a_{ff} . Although fits using third-order and fourth-order polynomials agree on the central value, the former yields a smaller error bar. The final results for the effective range is $r_{\text{dd}}/a_{\text{ff}} = -0.413(79)$. In Table II we show the results from the constrained fit.

TABLE II: The results from the constrained fit for the dimer-dimer effective range.

$c_{3N,4N}$	$f_0 = r_{\text{dd}}/a_{\text{ff}}$	f_1	f_2	f_3
0.00	-0.413±0.079	6.536±3.158	11.197±8.264	-12.085±5.365
0.02		7.062±2.900	-8.163±7.885	5.224±5.239
0.06		7.074±2.137	-8.166±5.674	3.675±3.710
0.10		7.555±1.775	-10.036±4.638	4.526±3.003
0.12		7.518±1.598	-10.273±4.166	4.649±2.697
0.16		1.445±0.559	-0.508±1.383	0.288±0.953
0.20		1.598±0.463	-0.836±0.953	0.450±0.619
0.40		1.329±0.434	0.457±0.815	-0.619±0.494
0.60		1.363±0.418	0.496±0.728	-0.671±0.412
0.80		1.461±0.400	0.334±0.678	-0.581±0.375
1.00		1.457±0.385	0.401±0.625	-0.626±0.333
1.20		1.556±0.395	0.215±0.632	-0.518±0.326
1.40		1.578±0.398	0.217±0.630	-0.531±0.319
1.60		1.582±0.397	0.241±0.625	-0.547±0.316
1.80		1.612±0.395	0.259±0.627	-0.587±0.320

V. SUMMARY AND CONCLUSIONS

In order to benchmark our numerical lattice methods, we first did a study of the fermion-dimer scattering for two-component fermions interacting via an attractive zero-range interaction on a periodic cubic lattice. We found excellent agreement with previous calculations of fermion-dimer scattering length a_{fd} and effective range r_{fd} . We then used the same methods to calculate the dimer-dimer scattering. We computed dimer-dimer scattering state energies and these were used to determine dimer-dimer scattering phase shifts via Lüscher’s finite volume method. These phase shifts were used to extract the dimer-dimer scattering length a_{dd} and effective range r_{dd} . We then performed continuum limit extrapolations for a_{dd} and r_{dd} .

In the dimer-dimer system, we found very large corrections to the effective range due to the lattice spacing, which made the determination of the effective range difficult. To overcome this challenge, we introduced three-body ($3N$) and four-body ($4N$) interactions. In the continuum limit these operators become irrelevant, however, they are very useful in producing additional data which can be used to determine the scattering parameters more accurately. We also found that the higher-body forces can be used to empirically cancel large lattice spacing corrections to the dimer-dimer effective range. This provided an advantage in the determination of the dimer-dimer effective range. We have found $a_{\text{dd}}/a_{\text{ff}} = 0.645 \pm 0.089$ and $r_{\text{dd}}/a_{\text{ff}} = -0.413 \pm 0.079$. This calculated scattering length is consistent with the known previous results for the dimer-dimer scattering length [4–7]. Our value for the effective range differs from previous results [9, 10], however it is our understanding that these calculations can be improved. In the case of Ref. [10], we have found that there are large lattice artifacts which produce a large positive dimer-dimer effective range at nonzero lattice spacing and have shown that including higher-body operators can greatly reduce this problem.

Our results should have immediate applications to the universal physics of shallow dimers. One particularly useful application is in the determination of the ground state energy density of a dilute gas of shallow dimers. The dimers behave as weakly-interacting repulsive Bose particles, and the energy density has been determined up to order ρa_{dd}^3 [17–20] as well as the first correction proportional to $r_{\text{dd}}/a_{\text{dd}}$ [21].

ACKNOWLEDGMENTS

The authors thank partial support from the U.S. National Science Foundation grant No. PHY-1307453, the DFG (SFB/TR 110, “Symmetries and the Emergence of Structure in QCD”) and the BMBF (contract No. 05P2015 - NUSTAR R&D). The work of UGM was supported in part by The Chinese Academy of Sciences (CAS) President’s International Fellowship Initiative (PIFI) grant no. 2015VMA076. Computing resources were provided by the Higher Performance Computing centers at Mississippi State University, North Carolina State University and RWTH Aachen.

-
- [1] W. Zwerger, ed., *The BCS-BEC Crossover and the Unitary Fermi Gas*, Lecture Notes in Physics, (Springer, 2012).
- [2] P. F. Bedaque and U. van Kolck, Phys. Lett. B **428**, 221 (1998) [nucl-th/9710073].
- [3] J. W. Chen, G. Rupak and M. J. Savage, Nucl. Phys. A **653**, 386 (1999) [nucl-th/9902056].
- [4] D. S. Petrov, C. Salomon and G. V. Shlyapnikov, Phys. Rev. Lett. **93**, 090404 (2004).
- [5] D. S. Petrov, C. Salomon and G. V. Shlyapnikov, Phys. Rev. A **71**, 012708 (2005) [cond-mat/0407579 [cond-mat.stat-mech]].
- [6] J. P. D’Incao, S. T. Rittenhouse, N. P. Mehta and C. H. Greene, Phys. Rev. A **79**, 030501 (2009).
- [7] A. Bulgac, P. F. Bedaque and A. C. Fonseca, (2003), arXiv:cond-mat/0306302 [cond-mat].
- [8] G. Rupak, nucl-th/0605074.
- [9] J. von Stecher, C. H. Greene and D. Blume, Phys. Rev. A **76**, 053613 (2007).
- [10] D. Lee, Eur. Phys. J. A **35**, 171 (2008) [arXiv:0704.3439 [cond-mat.supr-con]].
- [11] M. Lüscher, Commun. Math. Phys. **105**, 153 (1986). doi:10.1007/BF01211097
- [12] M. Lüscher, Nucl. Phys. B **354**, 531 (1991).
- [13] S. Bour, S. Koenig, D. Lee, H.-W. Hammer and U.-G. Meißner, Phys. Rev. D **84**, 091503 (2011) [arXiv:1107.1272 [nucl-th]].
- [14] F. Gabbiani, P. F. Bedaque and H. W. Griefhammer, Nucl. Phys. A **675**, 601 (2000) [nucl-th/9911034].
- [15] P. F. Bedaque, H. W. Hammer and U. van Kolck, Phys. Rev. C **58**, R641 (1998) [nucl-th/9802057].
- [16] P. F. Bedaque, G. Rupak, H. W. Griefhammer and H. W. Hammer, Nucl. Phys. A **714**, 589 (2003) [nucl-th/0207034].
- [17] T. D. Lee and C. N. Yang, Phys. Rev. **105**, 1119 (1957).
- [18] T. D. Lee, K. Huang, and C. N. Yang, Phys. Rev. **106**, 1135 (1957).
- [19] T. T. Wu, Phys. Rev. **115**, 1390 (1959).
- [20] E. Braaten, A. Nieto, Eur. Phys. J. B **11**, 143 (1999).
- [21] E. Braaten, H. W. Hammer, and S. Hermans, Phys. Rev. A **63**, 063609 (2001) [cond-mat/0012043].